

Singlet-doublet fermion dark matter with Dirac neutrino mass, $(g-2)_\mu$ and ΔN_{eff}

Debasish Borah,^{1,*} Satyabrata Mahapatra,^{2,†} Dibyendu Nanda,^{3,‡} Sujit Kumar Sahoo,^{4,§} and Narendra Sahu^{4,¶}

¹*Department of Physics, Indian Institute of Technology Guwahati, Assam 781039, India*

²*Department of Physics and Institute of Basic Science,
Sungkyunkwan University, Suwon 16419, Korea*

³*School of Physics, Korea Institute for Advanced Study, Seoul 02455, Korea*

⁴*Department of Physics, Indian Institute of Technology Hyderabad,
Kandi, Sangareddy 502285, Telangana, India*

Abstract

We study the possibility of generating light Dirac neutrino mass via scotogenic mechanism where singlet-doublet fermion dark matter (DM) plays non-trivial role in generating one-loop neutrino mass, anomalous magnetic moment of muon $(g-2)_\mu$ as well as additional relativistic degrees of freedom ΔN_{eff} within reach of cosmic microwave background (CMB) experiments. We show that the Dirac nature of neutrinos can bring interesting correlations within the parameter space satisfying the $(g-2)_\mu$ anomaly and DM relic density and the effective relativistic degrees of freedom ΔN_{eff} . While we stick to thermal singlet doublet DM with promising detection prospects, both thermal and non-thermal origin of ΔN_{eff} have been explored. In addition to detection prospects at DM, $(g-2)$ and other particle physics experiments, the model remains verifiable at future CMB experiments like CMB-S4, SPT-3G.

I. INTRODUCTION

The enduring enigmas of the cosmos have perpetually captivated the minds of physicists and researchers, propelling them on an unyielding quest to fathom the intricacies of its foundational structure and dynamics. Amid the multitude of puzzles that persist in challenging our comprehension, the most pivotal riddles are the identity of dark matter (DM) and its dynamics, genesis of neutrino mass and the long standing $(g-2)$ anomalies of the Standard Model (SM).

Dark matter stands as one of the most enigmatic mysteries, its presence inferred primarily through its gravitational effects on visible matter and cosmic structures. Despite its elusiveness, the remarkable realization that DM constitutes almost 85% of the total matter content and roughly 27% of the total energy density of the universe, from the satellite borne experiments like WMAP and PLANCK [1, 2], which measure anisotropies in CMB, has elevated it to be a pivotal cornerstone of cosmology. The current abundance of DM is frequently expressed in terms of the density parameter Ω_{DM} and the normalized Hubble parameter h , defined as the Hubble Parameter divided by $100 \text{ km s}^{-1} \text{ Mpc}^{-1}$, yielding $\Omega_{\text{DM}} h^2 = 0.120 \pm 0.001$ at a 68% C.L.. However, none of the conventional SM particles satisfy the criteria to serve as a plausible DM candidate. This has prompted the exploration of several beyond standard model (BSM) frameworks among which the weakly interacting massive particle (WIMP) paradigm stands as one of the extensively researched paradigms. Within the WIMP frame-

work, a potential DM particle candidate with mass and interaction strength of the order of the electroweak scale could yield the observed DM abundance through thermal freeze-out, a notable coincidence often termed the “WIMP Miracle”. The same interactions accountable for the thermal freeze-out of WIMPs also engender promising prospects for their direct detection at terrestrial laboratories. However, direct detection experiments have yet to detect such scattering events, consequently imposing more stringent constraints on the couplings between DM and nucleons. Analogous null outcomes have also been reported in indirect detection and collider experiments. A recent comprehensive assessment of WIMP-type DM models is available in a recent review [3, 4]. The absence of positive results in WIMP detection has also spurred the particle physics community to explore alternative and complementary avenues of investigation.

In addition to its limitations regarding DM, the SM also falls short in explaining the origin of neutrino mass and mixing, confirmed through neutrino oscillation experiments[5–9]. The oscillation data exclusively captures differences in mass-squared values, while the absolute mass scale is constrained to $|\sum_i m_{\nu_i}| \leq 0.12 \text{ eV}$ based on cosmological observations [1]. Despite compelling evidence pointing towards nonzero neutrino masses, a critical question remains unanswered: the intrinsic nature of neutrinos, whether they are of the Dirac or Majorana type. While neutrino oscillation experiments are unable to definitively resolve this matter, other experimental avenues, such as searches for neutrino-less double beta decay ($0\nu\beta\beta$), hold the potential to confirm the Majorana nature of neutrinos. To date, we have no such evidence, leaving the Majorana nature of light neutrinos unverified. This has kindled increased interest in exploring the plausibility of light Dirac neutrinos. While traditional Dirac neutrino mass models built on the seesaw mechanism have been discussed in [10–12], alternative scenarios outlining the possibility of light Dirac neu-

*Electronic address: dborah@iitg.ac.in

†Electronic address: satyabrata@g.skku.edu

‡Electronic address: dnanda@kias.re.kr

§Electronic address: ph21resch11008@iith.ac.in

¶Electronic address: nsahu@phy.iith.ac.in

trino mass can be found in [13–15] and related references.

Apart from DM and neutrino mass, another long-standing puzzle challenging the phenomenological success of SM is the anomalous magnetic moment of muon, commonly denoted as a_μ . This refers to the deviation between its measured magnetic moment and the theoretically predicted value within SM. The significance of a_μ lies in its sensitivity to both known and unknown particle interactions, rendering it a crucial testing ground for new physics beyond the SM. The 2021 analysis conducted by the Muon $g-2$ collaboration, with the Fermilab’s E989 experiment result in conjunction with the prior results from Brookhaven, revealed a discrepancy of 4.2σ . A more recent analysis by the same collaboration [16] has yielded $\Delta a_\mu = a_\mu^{\text{exp}} - a_\mu^{\text{SM}} = 249(48) \times 10^{-11}$, indicating a discrepancy of 5.1σ at confidence level. It is important to note that, due to the non-perturbative nature of the low-energy strong interaction, the uncertainty in a_μ^{SM} is primarily dominated by contributions from hadronic vacuum polarization (HVP). These contributions are derived from data-driven methodologies, utilizing experimentally obtained $e^+e^- \rightarrow \text{hadrons}$ data or from Lattice Quantum Chromodynamics (QCD) computations. Results from various lattice groups are combined using a conservative approach to provide an average leading-order (LO) value of $a_\mu^{\text{LO HVP}} = 711.6(18.4) \times 10^{-10}$ [17] and this has been measured with even greater precision by the recent CMD-3 experiment [18]. While these observations contribute to alleviating the tension between the experimental value of a_μ and its SM prediction, they do not provide any conclusive evidence yet, keeping BSM explanations viable. Review of such new physics explanations for muon $(g-2)$ can be found in [19–21].

While the origin of these puzzles is hitherto unknown, it is appealing and instructive to seek a theory that can explain them in a common framework with interesting detection prospects. This article endeavors to formulate a concise model capable of offering a plausible dark matter explanation for the Universe while concurrently addressing the issues of neutrino mass and muon $g-2$. We study a WIMP-like fermionic dark matter scenario involving a vector-like singlet and a doublet. The rationale for exploring this particular fermionic configuration is well-established as in singlet-doublet setups, there is mixing between the neutral component of the doublet and the singlet through the Yukawa interaction and DM manifests as a mixed state, satisfying appropriate relic density across a broad range of masses while adhering to direct search limits, which is not the case for a purely singlet or doublet scenario [22–50]. The singlet-doublet fermionic DM has already been considered in literature in connection to Majorana neutrino masses [47–51]. Here we consider a minimal extension of this model with the inclusion of one additional Z_2 odd scalar and 3 RHNs (ν_{R_i}) to incorporate the Dirac mass of light neutrinos in a scotogenic setup, which also leads to complementary cosmological probes of the scenario [32–40].

As the genesis of Dirac neutrino mass demands the

presence of right chiral components, such scenarios have the potential to introduce extra relativistic degrees of freedom, often referred to as dark radiation. These additional degrees of freedom can be explored through CMB experiments [1, 2]. Current CMB constraints have placed limitations on effective neutrino degrees of freedom during the recombination era ($z \sim 1100$), yielding $N_{\text{eff}} = 2.99_{-0.33}^{+0.34}$ at 2σ or 95% confidence level, including baryon acoustic oscillation (BAO) data. This constraint becomes more stringent, leading to $N_{\text{eff}} = 2.99 \pm 0.17$ at the 1σ confidence level. Comparable bounds also arise from big bang nucleosynthesis (BBN), indicating $2.3 < N_{\text{eff}} < 3.4$ at the 95% confidence level. These constraints are in alignment with the SM predictions of $N_{\text{eff}}^{\text{SM}} = 3.046$. However, future experiments such as CMB Stage IV (CMB-S4) [52] are anticipated to achieve unprecedented sensitivity, aiming to reach $\Delta N_{\text{eff}} = N_{\text{eff}} - N_{\text{eff}}^{\text{SM}} = 0.06$ at 2σ , thereby approaching the SM prediction. This enhanced precision holds the potential to scrutinize the BSM scenarios featuring light degrees of freedom that were once in equilibrium with the SM or were non-thermally generated through the decay or annihilation of heavier species. Recently, in [53], the possibility of observable ΔN_{eff} in a Dirac scotogenic model with additional scalar doublet was studied. However, the present setup comes with the advantage of providing an explanation for $(g-2)_\mu$ as well, details of which we discuss in the upcoming sections.

Due to the minimality of the framework, which offers a unified resolution to the aforementioned challenges, and considering the array of supplementary phenomenological and experimental constraints, a robust correlation becomes apparent among the model parameters, making the model extremely prognostic at various present and future experiments. The rest of the paper is organized as follows. In section II, we discuss a most minimal extended version of the singlet-doublet fermionic model to incorporate Dirac neutrino mass. In section III, we show the generation of Dirac neutrino mass at one-loop level. In section IV, we analyse the bounds of muon $(g-2)$ on our model parameters followed by the lepton flavour violation constraint. In section V, we discuss the relic density of DM and direct detection. In section VI, we discuss the details of ΔN_{eff} and finally conclude in section VII.

II. THE MODEL

We augment the SM fermion content by adding N copies of vector-like fermion doublet $\Psi = (\psi^0 \psi^-)^T$ (with hypercharge $Y = -1$, where we use $Q = T_3 + Y/2$) and N copies of vector-like singlet fermion χ , together with three copies of right handed neutrino ν_R which constitute the right chiral parts of light Dirac neutrinos. Both Ψ, χ are odd under an unbroken Z_2 symmetry which guarantees the stability of the lightest Z_2 -odd particle. In order to generate light neutrino data [54], we require $N \geq 2$. In addition to the minimal singlet doublet fermionic exten-

sion of SM, we introduce another singlet scalar ϕ , which is also odd under the Z_2 symmetry. A softly broken Z_3 symmetry is imposed to forbid the tree-level Dirac neutrino mass. The charge assignment of the particles under the imposed symmetry is shown in Table. I.

Gauge Group	Fermion Fields				Scalar
	L	Ψ	χ	ν_R	ϕ
$SU(2)_L$	2	2	1	1	1
$U(1)_Y$	-1	-1	0	0	0
Z_3	ω	ω^2	ω^2	ω^2	1
Z_2	+1	-1	-1	+1	-1

TABLE I: Particles and their charge assignments in our setup.

The relevant Lagrangian of the model guided by imposed symmetry is given by:

$$\begin{aligned} \mathcal{L} \supset & i\bar{\Psi}\gamma^\mu D_\mu\Psi + i\bar{\chi}\gamma^\mu\partial_\mu\chi - M_\Psi\bar{\Psi}\Psi - M_\chi\bar{\chi}\chi \\ & - y\bar{\Psi}\tilde{H}\chi - \lambda_\psi\bar{L}\phi\Psi - \lambda_\chi\bar{\nu}_R\phi\chi + h.c. \end{aligned} \quad (1)$$

Where $D_\mu = \partial_\mu - g_1\frac{\tau_i}{2}W_\mu^i - g_2\frac{Y}{2}B_\mu$, L is the lepton doublet and H is the SM Higgs doublet. Here we have suppressed the generation indices. We assign a charge of ω under the Z_3 symmetry to the SM leptons. Consequently, the term $\lambda_\psi\bar{L}\phi\Psi$ introduces a soft breaking of the Z_3 symmetry. This soft breaking proves essential for generating light neutrino mass through a one-loop mechanism, as will be elaborated in the next section. An alternative way of breaking Z_3 softly is to upgrade ϕ to a complex scalar with non-zero Z_3 charge and introduce a soft $\mu_\phi^2\phi^2$ term. One can also introduce another singlet scalar to break Z_3 spontaneously. While such spontaneous discrete symmetry breaking can have other cosmological issues like domain walls, our generic conclusions do not change on the details of Z_3 breaking. In the spirit of minimality, we, therefore, stick to the softly broken Z_3 mentioned above.

The scalar potential of the model involving ϕ is given by:

$$\begin{aligned} V_{H,\phi} = & -\mu_H^2(H^\dagger H) + \lambda_H(H^\dagger H)^2 \\ & + \frac{M_\phi^2}{2}\phi^2 + \frac{\lambda_\phi}{4!}\phi^4 + \lambda_{\phi H}\phi^2(H^\dagger H) \end{aligned} \quad (2)$$

After electroweak symmetry breaking, when SM Higgs acquires a VEV, it leads to mixing between the neutral component of doublet ψ^0 and χ giving rise to two singlet-doublet admixed mass eigen states. The mass terms for

these fields can then be written together as follows:

$$\begin{aligned} -\mathcal{L}_{mass}^{VF} = & M_\Psi\bar{\psi}^0\psi^0 + M_\Psi\psi^+\psi^- + M_\chi\bar{\chi}\chi \\ & + \frac{yv}{\sqrt{2}}\bar{\psi}^0\chi + \frac{yv}{\sqrt{2}}\bar{\chi}\psi^0 \\ = & \begin{pmatrix} \psi^0 & \chi \end{pmatrix} \begin{pmatrix} M_\Psi & yv/\sqrt{2} \\ yv/\sqrt{2} & M_\chi \end{pmatrix} \begin{pmatrix} \psi^0 \\ \chi \end{pmatrix} \\ & + M_\Psi\psi^+\psi^-. \end{aligned} \quad (3)$$

Denoting the mass eigenstates as χ_1 and χ_2 and θ to be the mixing angle, the flavour basis, $(\psi^0 \ \chi)^T$ is related to the physical basis, $(\chi_1 \ \chi_2)^T$ through the unitary transformation:

$$\begin{pmatrix} \psi^0 \\ \chi \end{pmatrix} = U \begin{pmatrix} \chi_1 \\ \chi_2 \end{pmatrix} = \begin{pmatrix} \cos\theta & -\sin\theta \\ \sin\theta & \cos\theta \end{pmatrix} \begin{pmatrix} \chi_1 \\ \chi_2 \end{pmatrix}, \quad (4)$$

where the mixing angle is given by:

$$\tan 2\theta = \frac{\sqrt{2}yv}{M_\Psi - M_\chi}. \quad (5)$$

So, after mass diagonalisation, the mass eigen values of the physical states are given by:

$$\begin{aligned} M_{\chi_1} &= M_\Psi \cos^2\theta + \frac{yv}{\sqrt{2}}\sin 2\theta + M_\chi \sin^2\theta, \\ M_{\chi_2} &= M_\Psi \sin^2\theta - \frac{yv}{\sqrt{2}}\sin 2\theta + M_\chi \cos^2\theta \end{aligned} \quad (6)$$

Here ϕ being odd under the Z_2 symmetry, does not acquire any vev, thus forbidding any mixing between ν_R and χ . Assuming a mass hierarchy among the Z_2 odd particles to be $M_\Psi > M_\phi > M_\chi$, guarantees the stability of the lightest Z_2 odd particle χ_2 which is dominantly a singlet fermion χ with a small admixture of the doublet fermion Ψ . Here it is worth noting that most of the phenomenological aspects of the model are dictated by the Yukawa interactions written in the second line of Eq. (1). These interactions are responsible for generating the Dirac neutrino mass at the one-loop level and also play a crucial role in governing the phenomenology of dark matter. Additionally, the interaction of charged leptons with ϕ and the charged doublet ψ^- contributes positively to the anomalous magnetic moment of leptons. As mentioned earlier, in order to satisfy the neutrino oscillation data, a minimum of two generations of singlet-doublet fermions is required. The consideration of multiple generations of singlet-doublet fermions is also motivated in the context of addressing the CDF-II W-mass anomaly, as explored recently in [50]. However, in our present work, the role of heavier generation of singlet-doublet fermions is only to generate the correct neutrino data. For rest of the phenomenology discussed here, we focus only on the lighter generation of singlet-doublet fermions. This choice is justified

by considering a mass difference of the order of $\mathcal{O}(10^3)$ GeV between the two generations. Consequently, the presence of the heavier generation has negligible impact on the DM phenomenology and the ΔN_{eff} analysis, as we disregard inter-generational mixing among these dark fermions. Furthermore, assuming maximal mixing between the singlet and doublet fermions of the heavier generation allows us to fine-tune the corresponding couplings to leptons to smaller values, while being consistent with the neutrino data. This ensures that any additional contribution from the heavier generation of singlet-doublet fermions to $(g-2)_\mu$ and lepton flavor violation (LFV) processes remain suppressed when compared to the contributions from the lighter generation.

Thus the relevant parameters of the model are the masses $\{M_{\chi_1}, M_{\chi_2}, M_{\psi^-}, M_\phi\}$, the mixing angle ($\sin\theta$), and the couplings $\{\lambda_\psi, \lambda_\chi\}$. These parameters collectively influence various aspects including the neutrino mass generation, additional contribution to muon magnetic moment, DM annihilation and co-annihilation dynamics as well as the thermalization of ν_R acting as dark radiation and providing additional complementary cosmological probe for this scenario in terms of ΔN_{eff} , which we discuss in details in the subsequent sections of this article.

III. DIRAC NEUTRINO MASS

In this scenario, the renormalizable Dirac neutrino mass operator $\bar{L}H\nu_R$ can be realized at one-loop level with the singlet-doublet fermions ($\chi_{1,2}$) and the singlet scalar ϕ running in the loop as shown in Fig. 1.

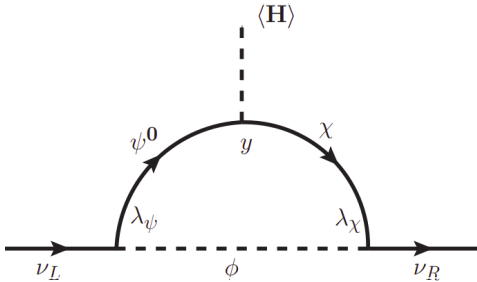


FIG. 1: Dirac Neutrino Mass generation at one-loop

The loop realization of the Dirac neutrino mass is shown in Fig. 1. Thus the light neutrino mass can be estimated to be [55]:

$$(m_\nu)_{\alpha\beta} = \frac{v}{4\pi^2} \sum_{i=1,2} (\lambda_\psi)_{\alpha i} y_i (\lambda_\chi)_{i\beta} F(M_{\chi_{1i}}, M_{\chi_{2i}}, M_\phi) \quad (7)$$

Where

$$F = [M_{\chi_1} M_{\chi_2} I_3(M_\phi, M_{\chi_1}, M_{\chi_2}) + J_3(M_\phi, M_{\chi_1}, M_{\chi_2})]$$

Here I_3 and J_3 are the loop integrals given in Appendix A.

Imposing the bound from cosmological data on the sum of light neutrino masses, $\sum m_i < 0.12$ eV, exerts a stringent constraint on the parameters governing the generation of the light Dirac neutrino mass. Assuming that the mass scale of the additional degrees of freedom is in the typical electroweak range ($\mathcal{O}(100)$ GeV), we derive an upper bound on the product $\lambda_\psi \lambda_\chi \theta$, which is $\lambda_\psi \lambda_\chi \theta < 10^{-10}$.

It is noteworthy that this constraint not only establishes a distinctive correlation between the neutrino mass and the muon $(g-2)$, but also forges intriguing links between the dark matter phenomenology and the model's predictions regarding ΔN_{eff} .

Model Parameters	Range for the scan
$\sin\theta$	$[10^{-8}, 1]$
λ_{ψ_α} ($\alpha = e, \mu, \tau$)	$[10^{-10}, 1]$
λ_{χ_β} ($\beta = e, \mu, \tau$)	$[10^{-10}, \sqrt{4\pi}]$
M_{χ_2}	$[1, 10^3]$ GeV
$\Delta M = M_{\chi_1} - M_{\chi_2}$	$[1, 10^3]$ GeV
$\Delta M_1 = M_\phi - M_{\chi_2}$	$[1, 600]$ GeV

TABLE II: Range of model parameters used for the numerical scan.

IV. MUON $(g-2)$ ANOMALY

The anomalous magnetic moment of the muon, often denoted as $g-2$, refers to the difference between the muon's actual magnetic moment and the value predicted by the Dirac equation within the framework of quantum electrodynamics (QED). This deviation arises due to quantum fluctuations and interactions with virtual particles in the vacuum.

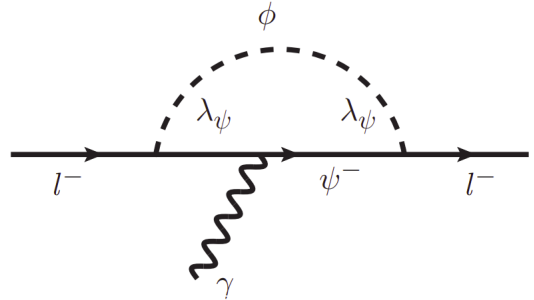


FIG. 2: Feynman diagram giving rise to muon $(g-2)$.

In our setup, the new positive contribution to the muon $g-2$ comes from the one loop diagram with the charged

doublet fermion ψ^- and the singlet scalar ϕ in the loop. This contribution to $(g-2)$ is given by[20],

$$\Delta a_\mu = \frac{\lambda_\psi^2 m_\mu^2}{8\pi^2 M_\phi^2} \int_0^1 dx \frac{x^2(1-x-\frac{M_\psi}{m_\mu})}{(1-x)(1-x\frac{m_\mu^2}{M_\phi^2})+x\frac{M_\psi^2}{M_\phi^2}} \quad (8)$$

In Fig. 3, we showcase the parameter space satisfying correct Δa_μ in the plane of λ_{ψ_μ} and M_{ψ^-} with the mass difference between M_{ψ^-} and M_ϕ in the colour code. We first carried out a numerical scan varying the model parameters in the range as shown in Table. II and find the parameter space that satisfies the correct neutrino mass criteria. The same parameter set is then used for the scan to check the constraint from $(g-2)_\mu$.

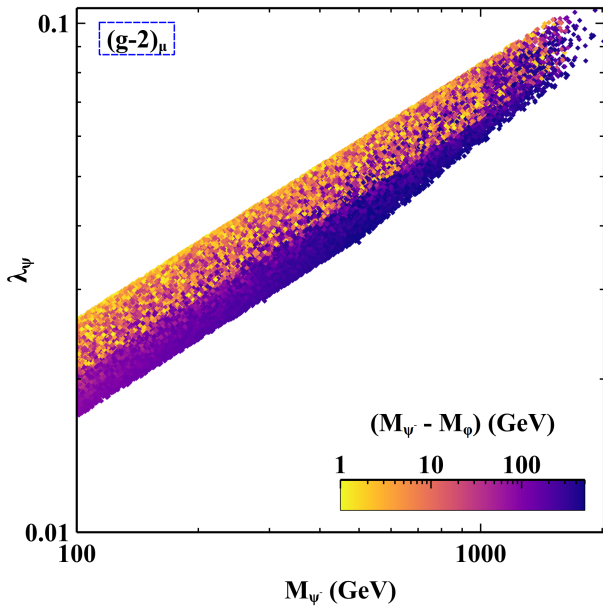


FIG. 3: The allowed region for Muon $(g-2)$ in the parameter space of M_{ψ^-} and λ_{ψ_μ} . The colour code is used for mass difference between ψ^- and ϕ

Clearly, we can see that λ_{ψ_μ} is constrained in the interval $[0.01, 0.1]$ while imposing the lower bound on the charged fermion doublet mass to be $M_{\psi^-} > 102.7$ GeV from LEP [56]. As, the mass of the particles in the loop suppresses the contribution to Δa_μ , the corresponding coupling λ_{ψ_μ} has to increase. Also the colour gradient shows that for smaller mass difference $(M_{\psi^-} - M_\phi)$, λ_{ψ_μ} is large and vice-versa.

A. Lepton Flavour Violation

The decay involving charged lepton flavour violation (CLFV) is a significant process for investigating physics beyond the SM. Within the SM framework, this process takes place at the one-loop level and is greatly suppressed due to the minuteness of neutrino masses, far beyond the

current experimental detection capabilities [57]. Consequently, any future detection of LFV decays, such as $\mu \rightarrow e\gamma$, would unquestionably constitute evidence of physics beyond the SM. In our current model, this additional new physics contribution comes from the same diagram as shown in Fig. 2 with leptons of two different flavours in the external legs. The decay width of $\mu \rightarrow e\gamma$ is given by:

$$\text{BR}(\mu^- \rightarrow e^- \gamma) = \frac{3\pi\alpha}{G_F^2} \lambda_{\psi_\mu} \lambda_{\psi_e} I(M_{\psi^-}, M_\phi) \quad (9)$$

Where

$$I(M_{\psi^-}, M_\phi) = \int_0^1 dx \int_0^{1-x} dy f(x, y, M_{\psi^-}, M_\phi)$$

And

$$f(x, y, M_{\psi^-}, M_\phi) = \frac{x(y+(1-x-y)\frac{m_e}{m_\mu})+(1-x)\frac{M_{\psi^-}}{m_\mu}}{-xyM_\mu^2-x(1-x-y)m_e^2+xM_\phi^2+(1-x)M_{\psi^-}^2}$$

Given the existing constraints on λ_{ψ_μ} and $M_{\psi^-, \phi}$ from the $(g-2)_\mu$ experiment, and taking into account the upper limit on $Br(\mu \rightarrow e\gamma)$ set by MEG [57], we establish an upper bound for λ_{ψ_e} . Upon conducting the analysis, we determine a conservative upper limit that λ_{ψ_e} must be less than 10^{-6} for $M_{\psi^-} \in [100, 1500]$ GeV in order to remain consistent with the MEG constraint.

V. DARK MATTER PHENOMENOLOGY

As outlined in section II, χ_2 , being the lightest Z_2 odd particle, attains stability and emerges as a plausible dark matter candidate in our framework. Being an admixed state of a singlet and a doublet fermion, its thermalization and relic abundance are crucially governed by the Yukawa and gauge interactions. Thus its relic density is determined by the process of thermal freeze-out, wherein the primary mechanisms involve the annihilation of dark matter into SM particles and ν_R , along with co-annihilation among the dark sector constituents χ_2 , χ_1 , ϕ , and ψ^- .

Before delving into the phenomenology of dark matter, it is important to note that the inclusion of ν_R and ϕ in this setup, and their significant involvement in the genesis of neutrino mass at one-loop, not only offers an additional cosmological probe to validate the model but also alters the conventional outcomes typically observed in the study of Dirac fermionic singlet-doublet DM as explored in [39, 44]. As in an upcoming section VI, we will thoroughly examine the ΔN_{eff} component of this scenario, it is pivotal to consider whether ν_R undergoes thermalization or not.

The production of RHNs (ν_{Ri}) primarily depends on the coupling parameter λ_χ . This same coupling also dictates whether RHNs undergo thermalization. For values of λ_χ greater than 10^{-3} , we observe that RHNs were in thermal equilibrium with the SM bath alongside other

constituents of the dark sector. Consequently, both ϕ annihilation and χ annihilation contribute to production of RHNs and hence enhancement of additional relativistic energy density. Conversely, for smaller values of λ_χ , RHNs were not in equilibrium with the SM bath, making it challenging to produce them through thermal processes. In such instances, RHNs can still be generated through non-thermal freeze-in processes, particularly via the decay of ϕ in the reaction $\phi \rightarrow \chi_2 \nu_R$.

Consequently, we categorize our analysis into two distinct cases:

- (i) **Case-1:** $10^{-3} < \lambda_\chi < \sqrt{4\pi}$.
- (ii) **Case-2:** $10^{-11} < \lambda_\chi \leq 10^{-3}$.

A. Relic Abundance of DM

The relic density of DM in this scenario is achieved by solving the Boltzmann equation

$$\frac{dn}{dt} + 3Hn = -\langle\sigma v\rangle_{\text{eff}}(n^2 - (n^{\text{eq}})^2) \quad (10)$$

where $n = \sum_i n_i$ represents the total number density of all the dark sector particles and n^{eq} is the equilibrium number density. $\langle\sigma v\rangle_{\text{eff}}$ represents the effective annihilation cross-section which takes into account all number changing process for DM freeze-out and this can be written as Eq.12, where g_1, g_2, g_3 and g_ϕ represent the internal degrees of χ_1, χ_2, ψ^- and ϕ respectively and Δ_i stands for the ratio $(M_i - M_{\chi_2})/M_{\chi_2}$ with M_i denoting the mass of χ_1, ψ^-, ϕ . Here g_{eff} is the effective degree of freedom which is given by:

$$g_{\text{eff}} = g_2 + g_\phi(1 + \Delta_\phi)^{3/2} \exp(-x\Delta_\phi) + g_1(1 + \Delta_{\chi_1})^{3/2} \exp(-x\Delta_{\chi_1}) + g_3(1 + \Delta_{\psi^-})^{3/2} \exp(-x\Delta_{\psi^-}) \quad (11)$$

and x is the dimensionless parameter M_{χ_2}/T .

$$\begin{aligned} \langle\sigma v\rangle_{\text{eff}} = & \frac{g_2^2}{g_{\text{eff}}^2} \langle\sigma v\rangle_{\chi_2\chi_2} + \frac{g_2 g_\phi}{g_{\text{eff}}^2} \langle\sigma v\rangle_{\chi_2\phi} (1 + \Delta_\phi)^{3/2} \exp(-x\Delta_\phi) + \frac{g_2 g_1}{g_{\text{eff}}^2} \langle\sigma v\rangle_{\chi_2\chi_1} (1 + \Delta_{\chi_1})^{3/2} \exp(-x\Delta_{\chi_1}) \\ & + \frac{g_2 g_3}{g_{\text{eff}}^2} \langle\sigma v\rangle_{\chi_2\psi^-} (1 + \Delta_{\psi^-})^{3/2} \exp(-x\Delta_{\psi^-}) + \frac{g_\phi^2}{g_{\text{eff}}^2} \langle\sigma v\rangle_{\phi\phi} (1 + \Delta_\phi)^3 \exp(-2x\Delta_\phi) \\ & + \frac{g_\phi g_1}{g_{\text{eff}}^2} \langle\sigma v\rangle_{\phi\chi_1} (1 + \Delta_\phi)^{3/2} (1 + \Delta_{\chi_1})^{3/2} \exp(-x(\Delta_\phi + \Delta_{\chi_1})) \\ & + \frac{g_\phi g_3}{g_{\text{eff}}^2} \langle\sigma v\rangle_{\phi\psi^-} (1 + \Delta_\phi)^{3/2} (1 + \Delta_{\psi^-})^{3/2} \exp(-x(\Delta_\phi + \Delta_{\psi^-})) \\ & + \frac{g_1^2}{g_{\text{eff}}^2} \langle\sigma v\rangle_{\chi_1\chi_1} (1 + \Delta_{\chi_1})^3 \exp(-2x\Delta_{\chi_1}) + \frac{2g_3^2}{g_{\text{eff}}^2} \langle\sigma v\rangle_{\psi^+\psi^-} (1 + \Delta_{\psi^-})^3 \exp(-2x\Delta_{\psi^-}) \\ & + \frac{g_1 g_3}{g_{\text{eff}}^2} \langle\sigma v\rangle_{\chi_1\psi^-} (1 + \Delta_{\chi_1})^{3/2} (1 + \Delta_{\psi^-})^{3/2} \exp(-x(\Delta_{\chi_1} + \Delta_{\psi^-})) \end{aligned} \quad (12)$$

The relic density of DM χ_2 can then be evaluated as :

$$\Omega_{\chi_2} h^2 = \frac{1.09 \times 10^9 \text{GeV}^{-1}}{\sqrt{g_*} M_{Pl}} \left[\int_{x_f}^{\infty} dx \frac{\langle\sigma v\rangle}{x^2} \right]^{-1} \quad (13)$$

Here $x_f = M_{\chi_2}/T_f$, and T_f denotes the freeze-out temperature of χ_2 .

To gain insight into the relic density of DM and the specific influence of model parameters in achieving the observed relic density, we conducted various analyses and explored the allowed parameter space. As studied in [38, 44], the pivotal parameters governing the relic abundance of a singlet-doublet Dirac fermionic DM include: the mass of the dark matter (M_{χ_2}), the mass splitting between the dominant singlet and dominant doublet physical states ($\Delta M = M_{\chi_1} - M_{\chi_2}$), and the mixing angle ($\sin\theta$). In addition to these three parameters, in the

present setup, we have additional parameters that also affect the relic density of DM because of the presence of ϕ and ν_R in the BSM particle spectrum. Presence of ϕ in the dark sector leads to additional co-annihilation processes where as ν_R facilitates new annihilation channel of DM to RHN. Thus the mass difference between ϕ and χ_2 , ($\Delta M_1 = M_\phi - M_{\chi_2}$), the scalar quartic coupling, $\lambda_{\phi H}$ as well as the DM ν_R Yukawa coupling with ϕ , λ_χ also become important parameters in determining the relic density of DM. So, in this model, we have a multi-dimensional parameter space that decides the relic density of DM. It is worth mentioning here that we used the package MicrOmegas [58] for computing annihilation cross-sections and relic density, after generating the model files using LanHEP [59].

In Fig. 4, we present the relic density of dark matter as

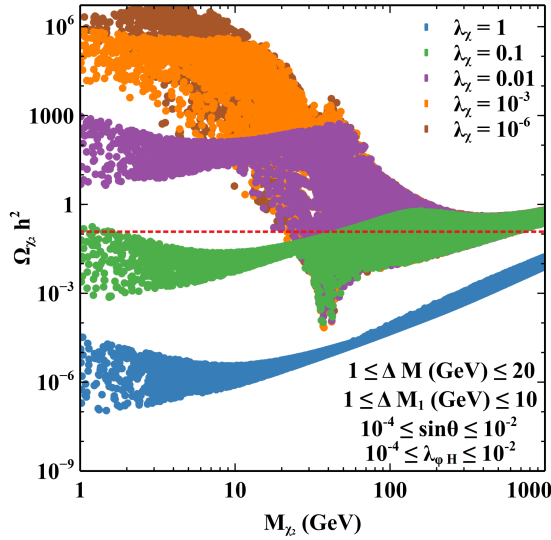


FIG. 4: Relic density of DM as a function of DM mass for different values of λ_χ , other parameters being varied randomly as mentioned in the inset.

a function of its mass, considering different benchmark values of λ_χ while randomly varying the other parameters ΔM , ΔM_1 , $\sin\theta$, and $\lambda_{\phi H}$ as shown in the inset of the figure. It is evident that an increase in λ_χ results in a gradual decrease in the relic density. This is attributed to the fact that as λ_χ increases, the annihilation cross-section of χ_2 into ν_R also increases. Consequently, the overall effective annihilation cross-section is enhanced, leading to a reduction in the relic density. Additionally, an interesting feature observed in Fig. 4 is that when λ_χ is not significantly large (i.e., $\lambda_\chi < 0.1$), the relic density of dark matter is influenced not only by its annihilation into ν_R , but also by other annihilation and co-annihilation processes involving SM particles mediated by the gauge bosons. This explains the resonance features observed around $M_V/2$ ($V \equiv W^\pm, Z$), represented by the green, purple, orange, and brown points. The Higgs resonance is not prominently visible in this plot because the Higgs-mediated annihilation or co-annihilation channels are less efficient for small $\sin\theta$ and small mass-splitting ΔM . This is attributed to the fact that the corresponding Yukawa coupling y is proportional to $\Delta M \times \sin\theta$, as illustrated in Eq. (5). However, in cases where λ_χ significantly surpasses other couplings, the channel $\chi_2\chi_2 \rightarrow \nu_R\nu_R$ becomes the predominant contributor to the relic density of χ_2 . Since this annihilation process occurs through a t -channel, resonance effects are not observed, as indicated by the blue points.

Fig. 5 illustrates the correlation between relic density and singlet and doublet mass splitting (ΔM), while mitigating the influence of dark matter annihilation to ν_{RS} by fixing $\lambda_\chi = 10^{-3}$. Other relevant parameters are varied randomly in a specific range as mentioned in the inset. With such a choice of parameters, DM annihilation to ν_R remains subdominant while the DM annihilation

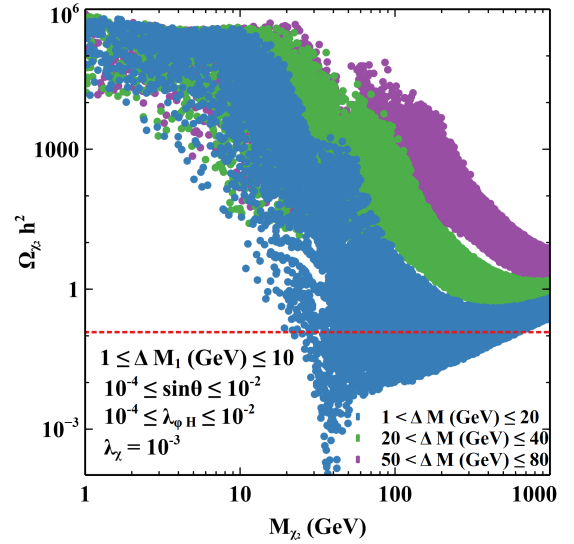


FIG. 5: Relic density of DM as a function of DM mass for different values of ΔM , other parameters being varied randomly as mentioned in the inset.

to SM particles and co-annihilation of DM with χ_1 and ψ^- dominantly decide the relic abundance. As we can see, with an increase in the mass-splitting ΔM , the relic density decreases and vice versa. This can be understood from Eq. (12) which is the effective annihilation cross-section of DM. As $\langle\sigma v\rangle_{\text{eff}}$ decreases with increase in $\Delta\chi_1 = \Delta M/M_{\chi_2}$ due to exponential suppression, which consequently elevates the relic density. It is important to note that Δ_{ψ^-} is not an independent parameter but rather is dependent on ΔM and $\sin\theta$.

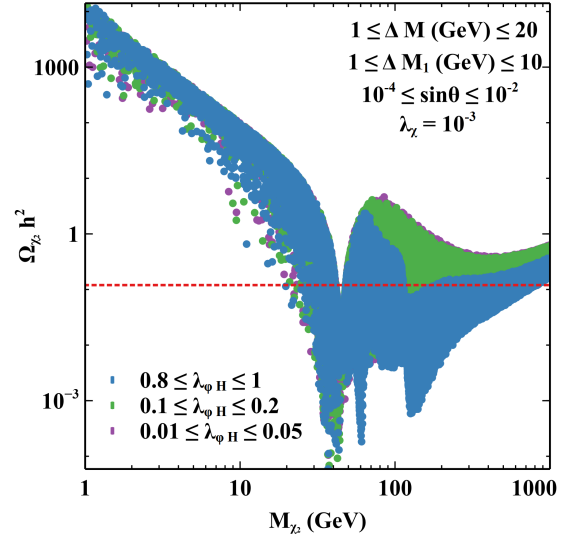


FIG. 6: Relic density as a function of DM mass for different ranges of $\lambda_{\phi H}$.

In Fig. 6, we depict $\Omega_{\chi_2} h^2$ as a function of M_{χ_2} for various selections of $\lambda_{\phi H}$ to demonstrate the depen-

density of relic density on this scalar quartic coupling. It is important to note that $\lambda_{H\phi}$ primarily affects the co-annihilation contribution in the effective annihilation cross-section, as it governs the rate of annihilation of ϕ as well as co-annihilation of ϕ and χ_2 to SM particles. For smaller values of $\lambda_{H\phi}$, we observe that the relic density is not very sensitive. It is only when $\lambda_{\phi H} \sim 1$ that this co-annihilation contribution becomes significant, ultimately influencing the relic density, as indicated by the blue points. The dips in the relic density correspond to resonances corresponding to gauge bosons and the SM Higgs boson.

A common feature observed in all three figures is that in the higher dark matter mass region, away from resonances, an increase in dark matter mass leads to a gradual rise in relic density. This phenomenon arises from the fact that in the non-relativistic limit, the effective annihilation cross-section of dark matter is inversely proportional to its mass. Consequently, as the dark matter mass increases, $\langle\sigma v\rangle_{\text{eff}}$ decreases, resulting in an increase in relic density.

B. Direct Detection

In this scenario, owing to the singlet-doublet mixing, the DM χ_2 can interact with the target nucleus in terrestrial direct search experiments through Z and Higgs mediated processes. This leads to the cross-section for Z -boson mediated dark matter-nucleon scattering to be: by [60, 61]

$$\sigma_{\text{SI}}^Z = \frac{G_F^2 \sin^4 \theta}{\pi A^2} \mu_r^2 \left| [Z f_p + (A - Z) f_n]^2 \right|^2 \quad (14)$$

Where the $f^p = f^n = 0.33$ correspond to the form factors for proton and neutron, respectively. Similarly, the spin-independent DM-nucleon scattering cross-section through Higgs mediation is given by:

$$\sigma_{\text{SI}}^h = \frac{4}{\pi A^2} \mu_r^2 \frac{y^2 \sin^2 2\theta}{M_h^4} \left[\frac{m_p}{v} \left(f_{Tu}^p + f_{Td}^p + f_{Ts}^p + \frac{2}{9} f_{TG}^p \right) + \frac{m_n}{v} \left(f_{Tu}^n + f_{Td}^n + f_{Ts}^n + \frac{2}{9} f_{TG}^n \right) \right]^2 \quad (15)$$

Different coupling strengths between DM and light quarks are given by [62, 63] as $f_{Tu}^p = 0.020 \pm 0.004$, $f_{Td}^p = 0.026 \pm 0.005$, $f_{Ts}^p = 0.014 \pm 0.062$, $f_{Tu}^n = 0.020 \pm 0.004$, $f_{Td}^n = 0.036 \pm 0.005$, $f_{Ts}^n = 0.118 \pm 0.062$. The coupling of DM with the gluons in target nuclei are parameterized by [64] $f_{TG}^n = 1 - \sum_{q=u,d,s} f_{Tq}^{p,n}$

Besides these tree-level processes for DM nucleon scattering, there exists another contribution to the spin-independent direct search cross-section, which arises at the loop level with ν_R and ϕ in the loop. The corresponding Feynman diagram is as shown in Fig. 7.

This cross-section can be evaluated as [65]:

$$\sigma_{\text{SI}}^{\text{loop}} = \frac{4}{\pi} \frac{M_{\chi_2}^2 m_p^2}{(M_{\chi_2} + m_p)^2} m_p^2 \mathcal{C}^2 f_q^2 \quad (16)$$

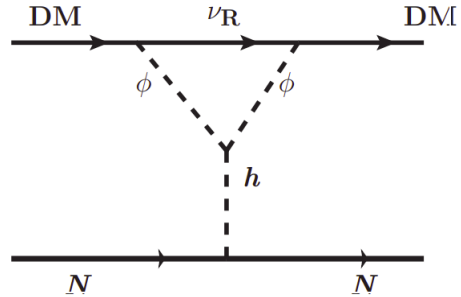


FIG. 7: Spin-independent elastic DM-nucleon scattering arising at one loop.

Where the form factor, $f_q \simeq 0.3$ and the loop-induced effective coupling, \mathcal{C} is given by,

$$\mathcal{C} = \frac{\lambda_\chi^2}{16\pi^2 M_h^2 M_{\chi_2}} \lambda_{\phi H} G \left(\frac{M_{\chi_2}^2}{M_\phi^2} \right)$$

And the loop function $G(x)$ is given by,

$$G(x) = \frac{x + (1-x)\ln(1-x)}{x}$$

From Eqs. (14), (15) and (16), it is clear that the DM-nucleon interaction strength crucially depends on $\sin \theta$ at tree level, and λ_χ and $\lambda_{\phi H}$ at loop level. Here, it is worth noting that, as λ_χ and $\sin \theta$ are correlated through the neutrino mass constraint as discussed in section. III, depending on their relative strength, the tree level or loop level contribution to DM-nucleon scattering dominates. We scrutinize the model parameters in both cases as mentioned at the beginning of section. V, against the most stringent constraint on DM-nucleon scattering cross-section from XENON-nT [66] and LZ [67] experiments and also showcase the projected sensitivity of the DARWIN experiment [68]. In case-1 ($\lambda_\chi > 10^{-3}$), because of loop-suppression $\sigma_{\text{SI}}^{\text{loop}}$, as well as because of very small $\sin \theta$, $\sigma_{\text{SI}}^{Z,h}$ remains far below the present sensitivity of LZ and Xenon-nT and hence most of the parameter space remains safe from the DM direct search bounds. This is visible from the upper panel of Fig. 8. In case-2 ($\lambda_\chi < 10^{-3}$), the one-loop contribution remains suppressed throughout and only the tree-level diagrams contribute to the DM-nucleon scattering. The bottom panel of Fig. 8 clearly illustrates that when $\sin \theta$ is substantial, the interaction strength is correspondingly high, resulting in a large DM-nucleon cross-section. As a result, direct search experiments impose significant constraints on $\sin \theta$. This stringent upper limit on $\sin \theta$ is $\sin \theta < 0.03$.

After incorporating the constraints from relic abundance and direct search of DM, now we show the final parameter space in the plane of DM mass and the mass-splittings ΔM and ΔM_1 for the two different cases

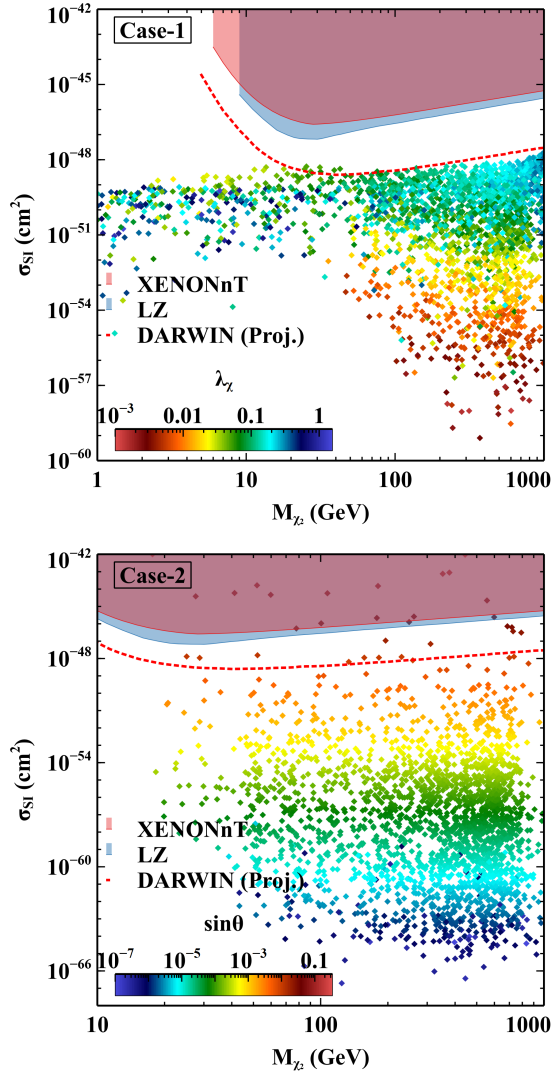


FIG. 8: Spin-independent DM-nucleon scattering cross-section as a function of DM mass for case-1(Top) and case-2(Bottom).

as mentioned earlier. We also impose the constraints from LEP experiment on the mass of the charged fermion doublet (M_{ψ^-}) *i.e.* $M_{\psi^-} > 102.7$ GeV. We also restrict the mass of ϕ to be greater than $M_H/2$ to avoid the constraints from Higgs invisible decay. In the following figures, Fig. 9-12, all the points shown satisfy the correct relic density, however, the grey coloured points are ruled out when we impose the above mentioned constraints.

Case-1 :

As we know in case-1, characterized by large value of λ_χ , the primary process determining the correct relic density of χ_2 is $\chi_2\chi_2 \rightarrow \nu_R\nu_R$ annihilation. Nevertheless, the contributions from co-annihilation, involving both ϕ annihilation to the SM and co-annihilation involving χ_1 and ψ^- , also play crucial roles. These contributions depend on the mass splittings ΔM_1 and ΔM . In Fig. 9, it is evi-

dent that as the mass splitting ΔM increases for smaller dark matter (DM) mass $M_{\chi_2} \lesssim 100$ GeV, λ_χ must also be raised to attain the correct relic density. This adjustment is necessary because with an increase in ΔM , the co-annihilation effect gradually diminishes, consequently reducing the effective cross section $\langle\sigma v\rangle_{\text{eff}}$. Therefore, an increase in λ_χ is required to offset this effect and achieve the correct relic density. In the region where $M_{\chi_2} \lesssim 100$ GeV and $\Delta M \lesssim 100$ GeV, most of the points shaded in grey are excluded due to the imposed constraint on M_{ψ^-} from the LEP experiment. As we increase the DM mass, we observe that in the lower mass-splitting region ($\Delta M \lesssim 15$ GeV), the mass splitting gradually decreases to achieve the correct relic density. This is because as the DM mass increases, the effective cross section $\langle\sigma v\rangle_{\text{eff}}$ decreases. Consequently, more co-annihilation contribution is required for compensation, necessitating a decrease in ΔM . The region below this always remains under-abundant. In the high DM mass region ($M_{\chi_2} \gtrsim 100$ GeV), it becomes evident that λ_χ does not necessarily have to be large. All values of λ_χ are permissible in this region. This is because even if λ_χ is small enough that DM annihilation to ν_R is not highly efficient, the relic density can still be brought to the correct range through various co-annihilation processes.

This understanding gains further support through an analysis of the results depicted in Fig. 10. By establishing a mass hierarchy among the particles in the dark sector as $M_{\chi_2} < M_\phi < M_{\chi_1}$, the co-annihilation processes involving ϕ exert a substantial influence in achieving the correct relic density. This influence is clearly evident in Fig. 10. Similar to the observations in Fig. 9, as the mass splitting $\Delta M_1 (= M_\phi - M_{\chi_2})$ increases, λ_χ must be augmented to offset the decrease in $\langle\sigma v\rangle_{\text{eff}}$ and thus attain the correct relic density. However, when ΔM_1 is small ($\Delta M_1 < 15$ GeV), λ_χ loses its significance, as the relic density is predominantly determined by the co-annihilation processes involving ϕ . This also clarifies the observed under-abundance in the region below $\Delta M \lesssim 15$ GeV in Fig. 9, since in this scenario, where $\Delta M_1 < \Delta M$, co-annihilation processes involving ϕ become overwhelmingly dominant, leading to a significant increase in $\langle\sigma v\rangle_{\text{eff}}$.

Case-2 :

In this case, λ_χ being very small ($\lambda_\chi < 10^{-3}$), it does not affect the relic density of DM. Rather, DM relic density is completely decided by the co-annihilation of DM with other dark sector particles. As discussed in section. VB, the stringent limit on $\sin\theta$ is $\sin\theta \lesssim 0.03$ to be consistent with the direct detection constraints. In the most minimal setup of fermionic singlet-doublet DM [38, 44], this crucially crunches the allowed parameter space to $\Delta M < 20$ GeV or so to satisfy correct relic density while being consistent with the direct detection constraints. However, in our setup, we get an enhanced parameter space as compared to this because of the additional channels involving ϕ that assist in achieving the

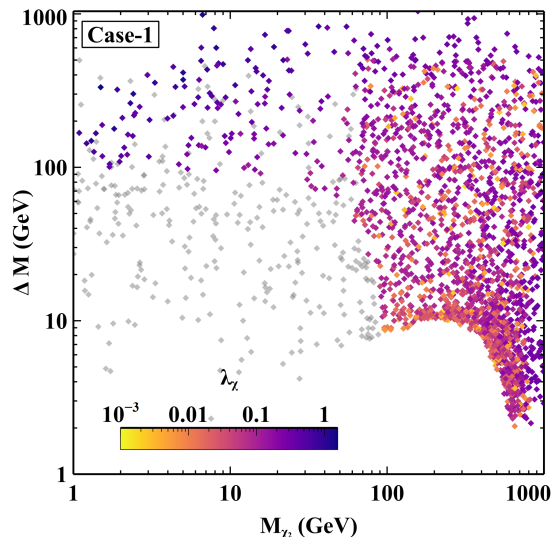


FIG. 9: Case-1: Correct relic density and direct detection constraint satisfying points in the plane of M_{χ_2} and ΔM . The color code depicts the value of λ_χ

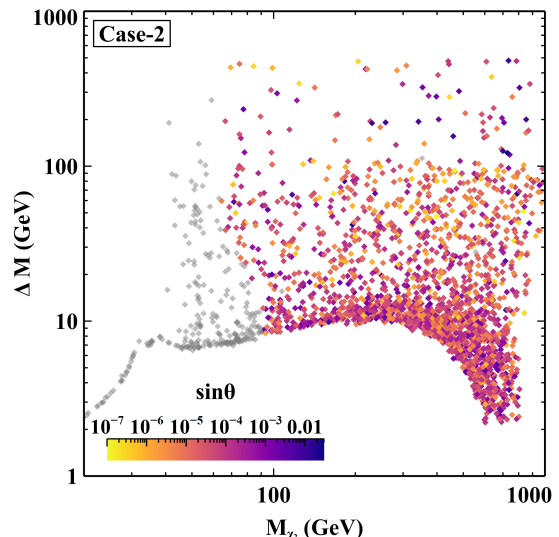


FIG. 11: Case-2: Correct relic density and direct detection constraint satisfying points in the plane of M_{χ_2} and ΔM . The color code depicts the value of $\sin\theta$

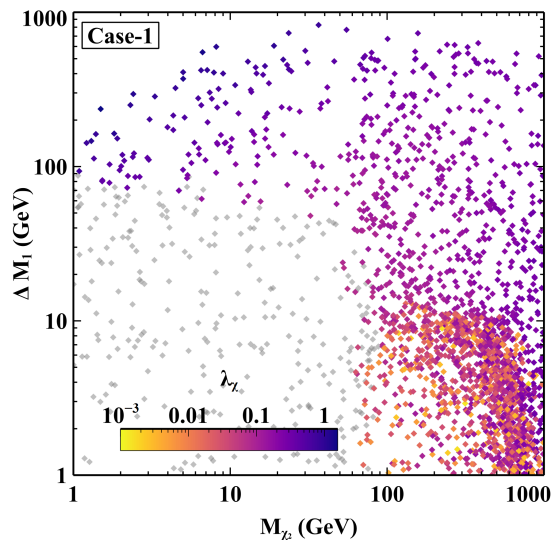


FIG. 10: Case-1: Correct relic density and direct detection constraint satisfying points in the plane of M_{χ_2} and ΔM_1 . The color code depicts the value of λ_χ

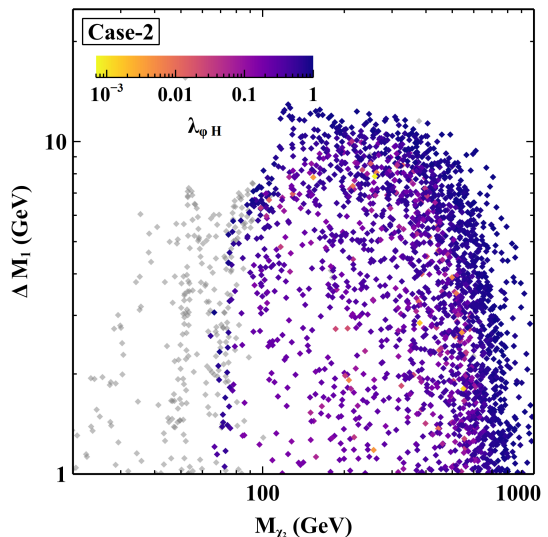


FIG. 12: Case-2: Correct relic density and direct detection constraint satisfying points in the plane of M_{χ_2} and ΔM_1 . The color code depicts the value of $\lambda_{\phi H}$.

correct relic density. Fig.11 depicts the co-annihilation effects of χ_1 and ψ^- where as Fig. 12 depicts the co-annihilation effects of ϕ . When $\sin\theta$ is small and ΔM is large, the singlet-doublet co-annihilation is not very effective but ϕ co-annihilation dominates over the singlet-doublet co-annihilation depending on $\lambda_{\phi H}$ coupling. It is evident from Fig. 12, that when $\lambda_{\phi H}$ is $\mathcal{O}(1)$, co-annihilations processes involving ϕ can significantly contribute to the correct relic density of DM.

VI. CONTRIBUTION TO ΔN_{eff}

Let us now focus on the phenomenological consequences that can occur due to the presence of the right-handed counterparts of the SM neutrinos. As mentioned in the earlier section, the Dirac nature of neutrinos necessitates the newly added right-chiral fermions to be as light as the left-handed SM neutrinos. The presence of such additional ultra-light species in the early universe can contribute substantially to the total radiation energy density and hence to the effective relativistic degrees of

freedom, N_{eff} which is usually parameterized as

$$N_{\text{eff}} \equiv \frac{\rho_{\text{rad}} - \rho_\gamma}{\rho_{\nu_L}}, \quad (17)$$

where ρ_{rad} is the total energy density of the thermal plasma whereas ρ_γ and ρ_{ν_L} are the energy density of photon and single active neutrino species respectively. Without the presence of any new light degrees of freedom, N_{eff} in SM have been calculated very precisely and quoted as 3.045¹ [69–72]. The current data from the observation of cosmic microwave background (CMB) by the Planck satellite [1] suggests $N_{\text{eff}} = 2.99_{-0.33}^{0.34}$ at 95% CL (including the baryon acoustic oscillation (BAO) data) which agrees with the SM prediction. The upcoming experiments such as CMB-S4 [52], SPT-3G [73] are expected to be extremely sensitive to N_{eff} and put much more stringent bounds than the Planck experiment due to their potential of exploring all the way down to $\Delta N_{\text{eff}} = N_{\text{eff}} - N_{\text{eff}}^{\text{SM}} = 0.06$.

Therefore, N_{eff} is a quantity of immense importance to test the presence of physics beyond SM which can affect CMB and is going to play a crucial role in our discussion. The significance of such contribution may vary depending on whether such light ν_R was present in the thermal bath or produced non-thermally [15, 74, 75]. The connection between the Dirac nature of neutrinos and the origin of DM production has been studied before in [10, 12] in the context of ΔN_{eff} . In this model, ν_R interacts only via Yukawa coupling $\lambda_\chi \bar{\nu}_R \phi \chi$ as shown in the Eq. (1). Hence, the production of ν_R , whether they were present in the thermal plasma or produced non-thermally with the evolution of our universe, solely depends on λ_χ . Here, we have studied both possibilities and calculated their contribution to ΔN_{eff} as mentioned by case-1 and case-2 in section V. From Eq. (17), the additional contribution to N_{eff} at the time of CMB coming from the presence of ν_R in the total radiation energy density can be written as,

$$\Delta N_{\text{eff}} = N_{\nu_R} \times \left. \frac{\rho_{\nu_R}}{\rho_{\nu_L}} \right|_{T=T_{\text{CMB}}}, \quad (18)$$

where N_{ν_R} is the number of relativistic ν_R , and ρ_{ν_R} is the energy density of the single ν_R . In the above equation, it is assumed that all three ν_R behave identically, hence contribute equally to the energy density. Depending on the production mechanism of ν_R we will discuss two following cases:

Case-1:

In this case, $\lambda_\chi > 10^{-3}$, the ν_R can be thermally produced in the early universe from the annihilation of χ and

ϕ . Fig. 13 shows the interactions responsible for keeping ν_R in equilibrium. Once these interaction rates dropped below the expansion rate of the universe, ν_R became decoupled from the thermal plasma and their temperature evolved independently. Hence by using entropy conservation in both sectors, one can write the excess contribution as

$$\Delta N_{\text{eff}} = N_{\nu_R} \times \left(\frac{T_{\nu_R}}{T_{\nu_L}} \right)^4 = N_{\nu_R} \left(\frac{g_{*s}(T_{\nu_L}^{\text{dec}})}{g_{*s}(T_{\nu_R}^{\text{dec}})} \right)^{4/3}, \quad (19)$$

where $g_{*s}(T)$ is the relativistic entropy degrees of freedom at temperature T , and T_{ν}^{dec} is the decoupling temperature of the species ν from the thermal bath. One important thing to keep in mind is that λ_χ also plays an important role in neutrino mass generation. Increasing λ_χ corresponds to a smaller mixing angle θ which corresponds to a weaker connection to the SM doublet ψ . While varying the parameters to find the viable parameter space we considered only those points that satisfy all possible constraints such as neutrino mass, muon $g-2$.

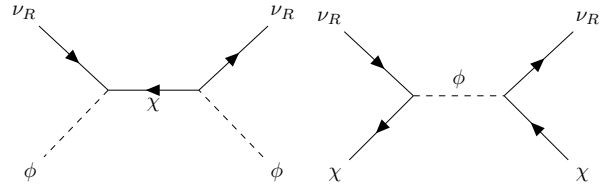


FIG. 13: Feynman diagram to keep ν_R in thermal equilibrium

Fig. 14 shows the variation of ΔN_{eff} as a function of DM mass ranging from 1 GeV to 1 TeV. The colour gradient shows the dependence on λ_χ . One can clearly see a correlation between ΔN_{eff} , λ_χ and the mass of DM. Larger λ_χ and lighter M_χ corresponds to larger contribution to the ΔN_{eff} . This can be understood as follows, larger λ_χ or lighter M_χ both forces χ and hence ν_R to be in thermal bath for longer time. The late decoupling of ν_R from the plasma decreases the denominator in Eq. (19) and increases its contribution to the N_{eff} . As discussed above, the yellow-shaded region is already excluded from the PLANCK 2018 data at 2σ CL. More importantly, future observations of microwave background can test this scenario fully as shown by the pink and orange dashed line, which corresponds to SPT-3G and CMB-IV, respectively. This is because once three of the ν_R s were produced in the thermal bath of the early universe, ΔN_{eff} would always have some minimum contribution of 0.14 which is well above the future prediction from CMB-S4 or SPT-3G. This is the manifestation of the conservation of entropy.

Case-2:

As discussed above, once the ν_R s or any light degrees of freedom were thermalized with the SM plasma,

¹ The deviation from 3 is due to various effects like non-instantaneous neutrino decoupling, flavour oscillations, and finite temperature QED corrections to the electromagnetic plasma [69–72].

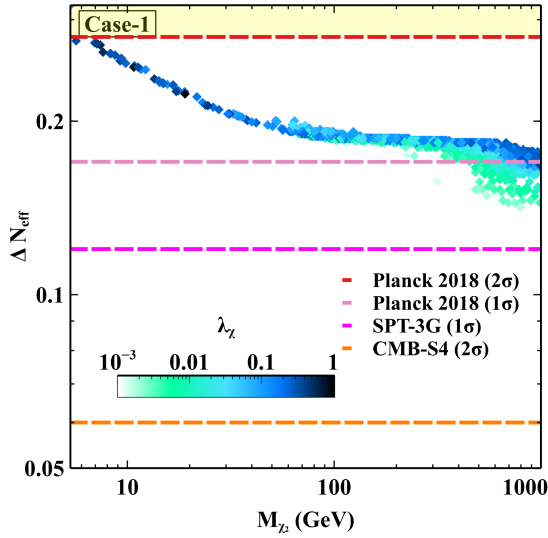


FIG. 14: ΔN_{eff} vs DM mass and the colour code is used for λ_χ . The dashed lines show experimental sensitivity, and the shaded region excluded by Planck 2018 with 2σ sensitivity.

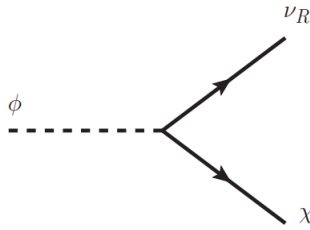


FIG. 15: Production of ν_R from the decay of ϕ

there would always be some minimum contribution to the ΔN_{eff} . However, this is not the same in case of non-thermal production. As we go to the smaller λ_χ , ν_R would no longer be produced in the thermal bath. Rather, they would produce from the decay of ϕ with a χ as shown in Fig. 15. In this case, we also need to track the evolution of ϕ as that will be important to calculate the total energy injected into the radiation energy in terms of light ν_R . We assume that ϕ was present in the thermal bath of the early universe and decays both from equilibrium and after freezing out from the thermal bath. So, to track the evolution of ν_R and ϕ we need to solve the following Boltzmann equations,

$$\frac{dY_\phi}{dx} = \frac{\beta s}{Hx} \left[-\langle \sigma v \rangle_{\phi\phi \rightarrow X\bar{X}} (Y_\phi^2 - (Y_\phi^{\text{eq}})^2) - \frac{\Gamma_\phi K_1(x)}{s K_2(x)} Y_\phi \right]$$

$$\frac{d\tilde{Y}_{\nu_R}}{dx} = \frac{\beta}{Hs^{1/3}x} \langle E\Gamma \rangle Y_\phi, \quad (20)$$

where the dimensionless parameters $Y_\phi = n_\phi/s$ and $\tilde{Y}_{\nu_R} = \rho_{\nu_R}/s^{4/3}$. In the above equation

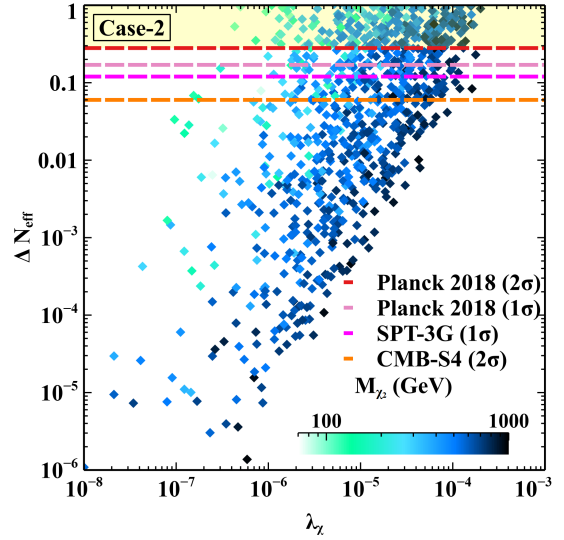


FIG. 16: ΔN_{eff} vs λ_χ . The colour code is shown for DM mass. Dashed lines show the experimental sensitivity and the shaded region is for the excluded region.

Γ_ϕ and $\langle E\Gamma \rangle$ can be expressed as

$$\Gamma(\phi \rightarrow \chi\nu_R) = \frac{1}{8\pi} \lambda_\chi^2 \cos^2 \theta^2 M_\phi \left(1 - \frac{M_{\chi_2}^2}{M_\phi^2} \right)^2 \quad (21)$$

$$\langle E\Gamma(\phi \rightarrow \chi\nu_R) \rangle = \frac{1}{16\pi} \lambda_\chi^2 \cos^2 \theta^2 M_\phi^2 \left(1 - \frac{M_{\chi_2}^2}{M_\phi^2} \right)^3 \quad (22)$$

$$\Delta N_{\text{eff}} = 3 \times 2 \left(\frac{\rho_{\nu_R}}{\rho_{\nu_L}} \right)_{T_D(\nu_L)}$$

$$= 2 \left(\frac{s^{4/3} \tilde{Y}_{\nu_R}}{\rho_{\nu_L}} \right)_{T_D(\nu_L)} \quad (23)$$

Once we solved the above Boltzmann equations, we used Eq. (23) to calculate the ΔN_{eff} produced by ρ_{ν_R} . The factor of 3 in Eq. (23) corresponds to the three generations of ν_R and 2 incorporates both particles and antiparticles. Fig. 16 shows the variation of ΔN_{eff} as a function of λ_χ where the colour bar represents the variation of M_χ . We have considered the mass difference between ϕ and χ to be ≤ 10 GeV. Eq. (22) says that with larger λ_χ , the decay width of ϕ will increase and hence more RHNs will be produced. If we increase the DM mass, the factor inside the bracket will decrease, hence the decay width will decrease. We can see ΔN_{eff} increases with λ_χ and for a fixed λ_χ , it decreases with increase in M_{χ_2} . One can note that some part of the parameter space is excluded from the present PLANCK data and future experiments can probe some part of it. However, for as we to the smaller λ_χ region, ΔN_{eff} becomes extremely small and drops well below the future projections of CMB-S4 or SPT-3G limits.

VII. CONCLUSION

In this study, we delved into a singlet-doublet fermionic dark matter model that offers a scotogenic avenue for generating Dirac neutrino masses. To achieve this, we extended the basic singlet-doublet dark matter framework by introducing an additional Z_2 -odd singlet scalar Φ and the right-chiral components of neutrinos, ν_R s. This extension also aids in addressing the muon $(g-2)$ anomaly, with a positive contribution arising from the one-loop diagram mediated by the charged fermion doublet ψ^- and ϕ . Following the inclusion of constraints stemming from neutrino mass, $(g-2)_\mu$, and lepton flavour violation (LFV), we conducted a comprehensive exploration of the dark matter phenomenology.

In the analysis of dark matter, we delineated two distinct cases for examination, based on the thermalisation criteria of ν_R , as this can yield intriguing implications from the perspective of the additional effective neutrino species (ΔN_{eff}). We find an enhanced parameter space because of the presence of ϕ in the dark sector as it helps in achieving correct relic density due to additional co-annihilation contributions. We considered both tree-level and loop-level DM-nucleon scattering possibilities for the DM direct detection perspectives. While direct dark matter search experiments do not impose stringent

restrictions on the model parameters, ΔN_{eff} offers an additional cosmological probe for the model. As ν_R is connected to the thermal bath, only through the dark sector particles, in the scenario, where ν_R is thermalized, future CMB experiment SPT-3G can probe the higher DM mass range of the model where as when ν_R is produced non-thermally, both SPT-3G and CMB-S4 can probe significant portion of the model parameter space.

Acknowledgments

The work of DB is supported by the Science and Engineering Research Board (SERB), Government of India grant MTR/2022/000575. SM acknowledges the financial support from the National Research Foundation of Korea grant 2022R1A2C1005050. The work of DN is supported by the National Research Foundation of Korea (NRF) grants, grant no. 2019R1A2C3005009(DN). DN also thanks the Department of Theoretical Physics, CERN where he was a visitor during the completion of the work. The work of NS is supported by the Department of Atomic Energy-Board of Research in Nuclear Sciences, Government of India (Ref. Number: 58/14/15/2021-BRNS/37220). SS would like to thank Pritam Das for useful discussion.

Appendix A: Loop Functions

$$\begin{aligned}
 I_3(M_\phi, M_{\chi_1}, M_{\chi_2}) &= \left[\frac{M_\phi^2 \ln \frac{M_{\chi_2}^2}{M_\phi^2}}{(M_\phi^2 - M_{\chi_1}^2)(M_\phi^2 - M_{\chi_2}^2)} + \frac{M_{\chi_1}^2 \ln \frac{M_{\chi_2}^2}{M_{\chi_1}^2}}{(M_{\chi_1}^2 - M_\phi^2)(M_{\chi_1}^2 - M_{\chi_2}^2)} \right] \\
 J_3(M_\phi, M_{\chi_1}, M_{\chi_2}) &= \left[A - \ln \left(\frac{M_{\chi_2}^2}{\text{GeV}^2} \right) + \frac{M_\phi^4 \ln \frac{M_{\chi_2}^2}{M_\phi^2}}{(M_\phi^2 - M_{\chi_1}^2)(M_\phi^2 - M_{\chi_2}^2)} + \frac{M_{\chi_1}^4 \ln \frac{M_{\chi_2}^2}{M_{\chi_1}^2}}{(M_{\chi_1}^2 - M_\phi^2)(M_{\chi_1}^2 - M_{\chi_2}^2)} \right]
 \end{aligned} \tag{A1}$$

where $A = \frac{2}{\epsilon} - \gamma_E + 1 + \ln 4\pi$

Appendix B: Lagrangian

Following from Eq. (1), we can write the Lagrangian in terms of physical states as,

$$\begin{aligned}
\mathcal{L}_{\text{int}}^{\text{DM}} &= i\bar{\Psi}\gamma^\mu(\partial_\mu - g\frac{\tau_i}{2}W_\mu^i - g'\frac{Y}{2}B_\mu)\Psi + i\bar{\chi}\gamma^\mu\partial_\mu\chi - (\lambda_\psi\bar{L}\phi\Psi + \lambda_\chi\bar{\nu}_R\phi\chi + \text{h.c.}) \\
\mathcal{L}_{\text{int}}^{\text{DM}} &= g_Z\left[\sin^2\theta\bar{\chi}_2\gamma^\mu Z_\mu\chi_2 + \cos^2\theta\bar{\chi}_1\gamma^\mu Z_\mu\chi_1 + \sin\theta\cos\theta(\bar{\chi}_1\gamma^\mu Z_\mu\chi_2 + \bar{\chi}_2\gamma^\mu Z_\mu\chi_1)\right] \\
&+ g_W(\sin\theta\bar{\chi}_2\gamma^\mu W_\mu^+\psi^- + \cos\theta\bar{\chi}_1\gamma^\mu W_\mu^+\psi^-) + g_W(\sin\theta\psi^+\gamma^\mu W_\mu^-\chi_2 + \cos\theta\psi^+\gamma^\mu W_\mu^-\chi_1) \\
&- g_Z c_{2w}\psi^+\gamma^\mu Z_\mu\psi^- - e_0\psi^+\gamma^\mu A_\mu\psi^- - \lambda_\psi\bar{e}_L\phi\psi^- \\
&- \left[\cos\theta(\lambda_\psi\bar{\nu}_L\phi\chi_1 + \lambda_\chi\bar{\nu}_R\phi\chi_2) + \sin\theta(\lambda_\chi\bar{\nu}_R\phi\chi_1 - \lambda_\psi\bar{\nu}_L\phi\chi_2)\right]
\end{aligned} \tag{B1}$$

where $g_Z = e_0/2s_w c_w$, $g_W = e_0/\sqrt{2}s_w$ and s_w, c_w, c_{2w} denote $\sin\theta_W$ and $\cos\theta_W$ and $\cos 2\theta_W$ respectively.

-
- [1] N. Aghanim et al. (Planck), *Astron. Astrophys.* **641**, A6 (2020), [Erratum: *Astron. Astrophys.* 652, C4 (2021)], 1807.06209, URL <https://doi.org/10.1051/0004-6361/201833910>.
- [2] G. Hinshaw et al. (WMAP), *Astrophys. J. Suppl.* **208**, 19 (2013), 1212.5226, URL <https://doi.org/10.1088/0067-0049/208/2/19>.
- [3] B. W. Lee and S. Weinberg, *Phys. Rev. Lett.* **39**, 165 (1977), URL <http://lss.fnal.gov/archive/1977/pub/Pub-77-041-T.pdf>.
- [4] K. Griest and M. Kamionkowski, *Phys. Rev. Lett.* **64**, 615 (1990), URL <https://lss.fnal.gov/archive/1989/pub/Pub-89-205-A.pdf>.
- [5] Y. Fukuda et al. (Super-Kamiokande), *Phys. Rev. Lett.* **81**, 1562 (1998), hep-ex/9807003, URL <https://science.energy.gov/hep/highlights/2015/hep-2015-11-a/>.
- [6] Q. R. Ahmad et al. (SNO), *Phys. Rev. Lett.* **87**, 071301 (2001), nucl-ex/0106015, URL <https://doi.org/10.1103/PhysRevLett.87.071301>.
- [7] Y. Abe et al. (Double Chooz), *Phys. Rev. Lett.* **108**, 131801 (2012), 1112.6353, URL <https://doi.org/10.1103/PhysRevLett.108.131801>.
- [8] F. P. An et al. (Daya Bay), *Phys. Rev. Lett.* **108**, 171803 (2012), 1203.1669, URL <https://doi.org/10.1103/PhysRevLett.108.171803>.
- [9] J. K. Ahn et al. (RENO), *Phys. Rev. Lett.* **108**, 191802 (2012), 1204.0626, URL <https://doi.org/10.1103/PhysRevLett.108.191802>.
- [10] A. Biswas, D. Borah, and D. Nanda, *JCAP* **10**, 002 (2021), 2103.05648, URL <https://doi.org/10.1088/1475-7516/2021/10/002>.
- [11] D. Borah, S. Mahapatra, D. Nanda, and N. Sahu, *Phys. Lett. B* **833**, 137297 (2022), 2204.08266, URL <https://doi.org/10.1016%2Fj.physletb.2022.137297>.
- [12] A. Biswas, D. Borah, N. Das, and D. Nanda, *Phys. Rev. D* **107**, 015015 (2023), 2205.01144, URL <https://doi.org/10.1103/PhysRevD.107.015015>.
- [13] D. Nanda and D. Borah, *Eur. Phys. J. C* **80**, 557 (2020), 1911.04703, URL <https://doi.org/10.1140/2Fepjc/2Fs10052-020-8122-4>.
- [14] D. Borah, S. Mahapatra, D. Nanda, and N. Sahu, *Phys. Lett. B* **811**, 135933 (2020), 2007.10754, URL <https://doi.org/10.1016%2Fj.physletb.2020.135933>.
- [15] A. Biswas, D. K. Ghosh, and D. Nanda, *JCAP* **10**, 006 (2022), 2206.13710, URL <https://doi.org/10.1088/2F1475-7516/2F2022/2F10/2F006>.
- [16] D. P. Aguillard et al. (Muon g-2) (2023), 2308.06230, URL <https://lss.fnal.gov/archive/2023/pub/fermilab-pub-23-385-ad-csaid-ppd.pdf>.
- [17] T. Aoyama et al., *Phys. Rept.* **887**, 1 (2020), 2006.04822, URL <https://doi.org/10.1016%2Fj.physrep.2020.07.006>.
- [18] F. V. Ignatov et al. (CMD-3) (2023), 2302.08834, URL <https://arxiv.org/pdf/2302.08834>.
- [19] F. Jegerlehner and A. Nyffeler, *Phys. Rept.* **477**, 1 (2009), 0902.3360.
- [20] M. Lindner, M. Platscher, and F. S. Queiroz, *Phys. Rept.* **731**, 1 (2018), 1610.06587, URL <https://doi.org/10.1016/j.physrep.2017.12.001>.
- [21] P. Athron, C. Balázs, D. H. J. Jacob, W. Kotlarski, D. Stöckinger, and H. Stöckinger-Kim, *JHEP* **09**, 080 (2021), 2104.03691.
- [22] A. Freitas, S. Westhoff, and J. Zupan, *JHEP* **09**, 015 (2015), 1506.04149, URL [https://doi.org/10.1007/JHEP09\(2015\)015](https://doi.org/10.1007/JHEP09(2015)015).
- [23] G. Cynolter, J. Kovács, and E. Lendvai, *Mod. Phys. Lett. A* **31**, 1650013 (2016), 1509.05323, URL <https://doi.org/10.1142/S0217732316500139>.
- [24] L. Calibbi, A. Mariotti, and P. Tziveloglou, *JHEP* **10**, 116 (2015), 1505.03867, URL [https://doi.org/10.1007/JHEP10\(2015\)116](https://doi.org/10.1007/JHEP10(2015)116).
- [25] T. Abe, R. Kitano, and R. Sato, *Phys. Rev. D* **91**, 095004 (2015), [Erratum: *Phys.Rev.D* 96, 019902 (2017)], 1411.1335, URL <https://doi.org/10.1103/PhysRevD.91.095004>.
- [26] C. Cheung and D. Sanford, *JCAP* **02**, 011 (2014), 1311.5896, URL <https://doi.org/10.1088/1475-7516/2014/02/011>.
- [27] T. Cohen, J. Kearney, A. Pierce, and D. Tucker-Smith, *Phys. Rev. D* **85**, 075003 (2012), 1109.2604, URL <https://doi.org/10.1103/PhysRevD.85.075003>.
- [28] R. Enberg, P. J. Fox, L. J. Hall, A. Y. Papaioannou, and M. Papucci, *JHEP* **11**, 014 (2007), 0706.0918, URL <https://doi.org/10.1088/1126-6708/2007/11/014>.
- [29] F. D'Eramo, *Phys. Rev. D* **76**, 083522 (2007), 0705.4493, URL <https://doi.org/10.1103/PhysRevD.76.083522>.
- [30] S. Banerjee, S. Matsumoto, K. Mukaida, and Y.-L. S.

- Tsai, JHEP **11**, 070 (2016), 1603.07387, URL [https://doi.org/10.1007/JHEP11\(2016\)070](https://doi.org/10.1007/JHEP11(2016)070).
- [31] A. Dutta Banik, A. K. Saha, and A. Sil, Phys. Rev. D **98**, 075013 (2018), 1806.08080, URL <https://doi.org/10.1103/PhysRevD.98.075013>.
- [32] S. Horiuchi, O. Macias, D. Restrepo, A. Rivera, O. Zapata, and H. Silverwood, JCAP **03**, 048 (2016), 1602.04788, URL <https://doi.org/10.1088/1475-7516/2016/03/048>.
- [33] D. Restrepo, A. Rivera, M. Sánchez-Peláez, O. Zapata, and W. Tangarife, Phys. Rev. D **92**, 013005 (2015), 1504.07892, URL <https://doi.org/10.1103/PhysRevD.92.013005>.
- [34] M. Badziak, M. Olechowski, and P. Szczerbiak, Phys. Lett. B **770**, 226 (2017), 1701.05869, URL <https://doi.org/10.1016/j.physletb.2017.04.059>.
- [35] A. Betancur, G. Palacios, and A. Rivera, Nucl. Phys. B **962**, 115276 (2021), 2002.02036, URL <https://doi.org/10.1016/j.nuclphysb.2020.115276>.
- [36] T. Abe, Phys. Lett. B **771**, 125 (2017), 1702.07236, URL <https://doi.org/10.1016/j.physletb.2017.05.048>.
- [37] T. Abe and R. Sato, Phys. Rev. D **99**, 035012 (2019), 1901.02278, URL <https://doi.org/10.1103/PhysRevD.99.035012>.
- [38] D. Borah, M. Dutta, S. Mahapatra, and N. Sahu, Phys. Rev. D **105**, 015029 (2022), 2109.02699, URL <https://doi.org/10.1103/PhysRevD.105.015029>.
- [39] S. Bhattacharya, N. Sahoo, and N. Sahu, Phys. Rev. D **96**, 035010 (2017), 1704.03417, URL <https://doi.org/10.1103/PhysRevD.96.035010>.
- [40] B. Barman, S. Bhattacharya, P. Ghosh, S. Kadam, and N. Sahu, Phys. Rev. D **100**, 015027 (2019), 1902.01217, URL <https://doi.org/10.1103/PhysRevD.100.015027>.
- [41] S. Bhattacharya, P. Ghosh, and N. Sahu, JHEP **02**, 059 (2019), 1809.07474, URL [https://doi.org/10.1007/JHEP02\(2019\)059](https://doi.org/10.1007/JHEP02(2019)059).
- [42] S. Bhattacharya, B. Karmakar, N. Sahu, and A. Sil, JHEP **05**, 068 (2017), 1611.07419, URL [https://doi.org/10.1007/JHEP05\(2017\)068](https://doi.org/10.1007/JHEP05(2017)068).
- [43] S. Bhattacharya, N. Sahoo, and N. Sahu, Phys. Rev. D **93**, 115040 (2016), 1510.02760, URL <https://doi.org/10.1103/PhysRevD.93.115040>.
- [44] S. Bhattacharya, P. Ghosh, N. Sahoo, and N. Sahu, Front. in Phys. **7**, 80 (2019), 1812.06505, URL <https://doi.org/10.3389/fphy.2019.00080>.
- [45] L. Calibbi, L. Lopez-Honorez, S. Lowette, and A. Mariotti, JHEP **09**, 037 (2018), 1805.04423, URL [https://doi.org/10.1007/JHEP09\(2018\)037](https://doi.org/10.1007/JHEP09(2018)037).
- [46] M. Dutta, S. Bhattacharya, P. Ghosh, and N. Sahu, Springer Proc. Phys. **277**, 685 (2022), 2106.13857, URL https://doi.org/10.1007/978-981-19-2354-8_124.
- [47] M. Dutta, S. Bhattacharya, P. Ghosh, and N. Sahu, JCAP **03**, 008 (2021), 2009.00885, URL <https://doi.org/10.1088/1475-7516/2021/03/008>.
- [48] P. Konar, A. Mukherjee, A. K. Saha, and S. Show, Phys. Rev. D **102**, 015024 (2020), 2001.11325, URL <https://doi.org/10.1103/PhysRevD.102.015024>.
- [49] P. Konar, A. Mukherjee, A. K. Saha, and S. Show, JHEP **03**, 044 (2021), 2007.15608, URL [https://doi.org/10.1007/JHEP03\(2021\)044](https://doi.org/10.1007/JHEP03(2021)044).
- [50] D. Borah, S. Mahapatra, and N. Sahu, Phys. Lett. B **831**, 137196 (2022), 2204.09671, URL <https://doi.org/10.1016/j.physletb.2022.137196>.
- [51] D. Borah, M. Dutta, S. Mahapatra, and N. Sahu, Phys. Rev. D **105**, 075019 (2022), 2112.06847, URL <https://doi.org/10.1103/PhysRevD.105.075019>.
- [52] K. Abazajian et al. (2019), 1907.04473, URL <https://lss.fnal.gov/archive/2019/pub/fermilab-pub-19-431-ae-scd.pdf>.
- [53] D. Borah, P. Das, and D. Nanda (2022), 2211.13168.
- [54] P. A. Zyla et al. (Particle Data Group), PTEP **2020**, 083C01 (2020).
- [55] E. Ma and O. Popov, Phys. Lett. B **764**, 142 (2017), 1609.02538, URL <https://doi.org/10.1016/j.physletb.2016.11.027>.
- [56] R. Barbieri, A. Pomarol, R. Rattazzi, and A. Strumia, Nucl. Phys. B **703**, 127 (2004), hep-ph/0405040, URL <https://doi.org/10.1016/j.nuclphysb.2004.10.014>.
- [57] A. M. Baldini et al. (MEG), Eur. Phys. J. C **76**, 434 (2016), 1605.05081.
- [58] G. Bélanger, F. Boudjema, A. Pukhov, and A. Semenov, Comput. Phys. Commun. **192**, 322 (2015), 1407.6129, URL <https://doi.org/10.1016/j.cpc.2015.03.003>.
- [59] A. Semenov, Comput. Phys. Commun. **180**, 431 (2009), 0805.0555, URL <https://doi.org/10.1016/j.cpc.2008.10.012>.
- [60] M. W. Goodman and E. Witten, Phys. Rev. D **31**, 3059 (1985), URL <https://doi.org/10.1103/PhysRevD.31.3059>.
- [61] R. Essig, Phys. Rev. D **78**, 015004 (2008), 0710.1668, URL <https://doi.org/10.1103/PhysRevD.78.015004>.
- [62] G. Bertone, D. Hooper, and J. Silk, Phys. Rept. **405**, 279 (2005), hep-ph/0404175, URL <https://doi.org/10.1016/j.physrep.2004.08.031>.
- [63] J. M. Alarcon, L. S. Geng, J. Martin Camalich, and J. A. Oller, Phys. Lett. B **730**, 342 (2014), 1209.2870, URL <https://doi.org/10.1016/j.physletb.2014.01.065>.
- [64] M. Hoferichter, P. Klos, J. Menéndez, and A. Schwenk, Phys. Rev. Lett. **119**, 181803 (2017), 1708.02245, URL <https://doi.org/10.1103/PhysRevLett.119.181803>.
- [65] A. Ibarra, C. E. Yaguna, and O. Zapata, Phys. Rev. D **93**, 035012 (2016), 1601.01163, URL <https://doi.org/10.1103/PhysRevD.93.035012>.
- [66] E. Aprile et al. (XENON), Phys. Rev. Lett. **131**, 041003 (2023), 2303.14729, URL <https://doi.org/10.1103/PhysRevLett.131.041003>.
- [67] D. S. Akerib et al. (LZ), Nucl. Instrum. Meth. A **953**, 163047 (2020), 1910.09124, URL <https://doi.org/10.1016/j.nima.2019.163047>.
- [68] J. Aalbers et al. (DARWIN), JCAP **11**, 017 (2016), 1606.07001, URL <https://doi.org/10.1088/1475-7516/2016/11/017>.
- [69] G. Mangano, G. Miele, S. Pastor, T. Pinto, O. Pisanti, and P. D. Serpico, Nucl. Phys. B **729**, 221 (2005), hep-ph/0506164, URL <https://doi.org/10.1016/j.nuclphysb.2005.09.041>.
- [70] E. Grohs, G. M. Fuller, C. T. Kishimoto, M. W. Paris, and A. Vlasenko, Phys. Rev. D **93**, 083522 (2016), 1512.02205, URL <https://doi.org/10.1103/PhysRevD.93.083522>.
- [71] P. F. de Salas and S. Pastor, JCAP **07**, 051 (2016), 1606.06986, URL <https://doi.org/10.1088/1475-7516/2016/07/051>.
- [72] M. Cielo, M. Escudero, G. Mangano, and O. Pisanti (2023), 2306.05460, URL <https://arxiv.org/pdf/2306.05460>.
- [73] J. S. Avva et al. (SPT-3G), J. Phys. Conf. Ser. **1468**, 012008 (2020), 1911.08047, URL <https://doi.org/10.1088/1751-8113/ab8047>.

- 1088/1742-6596/1468/1/012008.
- [74] X. Luo, W. Rodejohann, and X.-J. Xu, JCAP **06**, 058 (2020), 2005.01629, URL <https://doi.org/10.1088/1475-7516/2020/06/058>.
- [75] X. Luo, W. Rodejohann, and X.-J. Xu, JCAP **03**, 082 (2021), 2011.13059, URL <https://doi.org/10.1088/1475-7516/2021/03/082>.